Robust Surface States and Coherence Phenomena in Magnetically Alloyed SmB$_6$

Lin Miao,[1] Chul-Hee Min,[2] Yishuai Xu,[3] Zengle Huang,[4] Erica C. Kotta,[3] Rourav Basak,[3] M. S. Song,[5]
B. Y. Kang,[5] B. K. Cho,[5] K. Kißner,[2] F. Reinert,[2] Turgut Yilmaz,[6] Elio Vescovo,[6] Yi-De Chuang,[4]
Weida Wu,[4] Jonathan D. Denlinger,[7] and L. Andrew Wray[3],*

[1]School of Physics, Southeast University, Nanjing 211189, China
[2]Experimentelle Physik VII and Würzburg-Dresden Cluster of Excellence ct.qmat, Universität Würzburg,
Am Hubland, D-97074 Würzburg, Germany
[3]Department of Physics, New York University, New York, New York 10003, USA
[4]Rutgers Department of Physics and Astronomy, Rutgers University, Piscataway, New Jersey 08854, USA
[5]School of Materials Science and Engineering, Gwangju Institute of Science and Technology (GIST), Gwangju 61005, Korea
[6]National Synchrotron Light Source II, Brookhaven National Laboratory, Upton, New York 11973, USA
[7]Advanced Light Source, Lawrence Berkeley National Laboratory, Berkeley, California 94720, USA

Samarium hexaboride is a candidate for the topological Kondo insulator state, in which Kondo coherence is predicted to give rise to an insulating gap spanned by topological surface states. Here we investigate the surface and bulk electronic properties of magnetically alloyed Sm$_{1-x}M_x$B$_6$ (M = Ce, Eu), using angle-resolved photoemission spectroscopy and complementary characterization techniques. Remarkably, topologically nontrivial bulk and surface band structures are found to persist in highly modified samples with up to 30% Sm substitution and with an antiferromagnetic ground state in the case of Eu doping. The results are interpreted in terms of a hierarchy of energy scales, in which surface state emergence is linked to the formation of a direct Kondo gap, while low-temperature transport trends depend on the indirect gap.

The compound SmB$_6$ is a mixed-valence Kondo lattice system [1–3] that has been under intensive study since 2010 as a strong candidate for the topological Kondo insulator (TKI) state [4–6]. Angle-resolved photoemission (ARPES) measurements of the bulk band structure corroborate a TKI picture, in which dispersive 5d-orbital bands hybridize with semilocalized 4f-orbital states at the Fermi level to open a gap with topologically inverted symmetries [7–12]. Topologically associated surface states are seen to emerge as the gap opens at $T \sim 120$ K, and surface conductivity results in a low-temperature ($T < 10$ K) resistivity plateau. The bulk insulating behavior and surface conductivity are strikingly robust against fractional changes in stoichiometry and nonmagnetic alloying [13–15]; however, doping with magnetic elements (Ce, Gd) at a far lower ~1% level eliminates signatures of surface conductivity [13,14], consistent with the expectation that magnetic disorder will introduce backscattering and Anderson localization to the topological surface state system [16–18]. While these alloys represent fascinating extensions to the physics of the parent compound, Kondo latices are thought to be highly sensitive to disorder [37–39], and the fate of the TKI band structure in alloyed scenarios is unknown. Here, we report a comparative study of the electronic band structure, transport, and magnetic susceptibility properties of alloys incorporating small- and large-moment magnetic lanthanide

elements as Sm$_{1-x}M_x$B$_6$ (M = Ce, Eu). A clean low-temperature gap in the bulk 5d band is found to persist at the Fermi level up to the highest admixture levels tested (30% Ce, 20% Eu) and to be spanned by topologically associated surface states. The emergence of Fermi level topological surface states in samples with an antiferromagnetic ground state (Sm$_{1-x}$Eu$_x$B$_6$, $x \geq 0.1$) presents an antiferromagnetic topological insulator scenario [40,41] that has been much sought in recent years, with an advantage over other material candidates in that the topological band gap is positioned at the Fermi level. The physical conditions under which topological surface states emerge are found to remain tied to the *direct* 5d gap and to allow for a broad range of low-temperature resistivity trends defined by the *indirect* Kondo gap [42–44].

Single crystals of Sm$_{1-x}M_x$B$_6$ (M = Eu, Ce) were prepared by the alumina flux method and details of the sample growth are described in the Supplemental Material (Note 1 [18]). Multiple characterization methods, including x-ray diffraction, scanning tunneling microscope, and ultraviolet x-ray photoemission spectroscopy were performed, revealing homogeneous alloying within single-phase crystals with stoichiometry-consistent substitution on the lanthanide site (Supplemental Material, Note 2 [18]). Most ARPES measurements were performed at beam line 4.0.3 at the Advanced Light Source, with a base pressure better than 5×10^{-11} Torr.
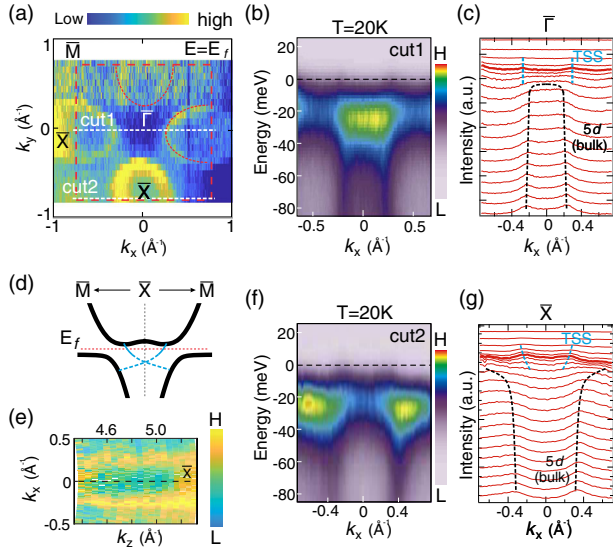
FIG. 1. Surface states after 30% Ce doping. (a) The Fermi surface of $Sm_{0.7}Ce_{0.3}B_6$, with dashed lines tracing ovoid surface state electron pockets. (b) A low-energy ARPES cut along the $\bar{X}$-$\bar{\Gamma}$-$\bar{X}$ momentum axis (cut 1). (c) Surface (blue) and bulk (black) bands are traced on momentum distribution curves from (b), with an energy step of 6 meV. (d) A band structure diagram showing (blue) a topological surface state and (black) hybridization-gapped bulk bands along the $\bar{M}$-$\bar{X}$-$\bar{M}$ axis. The lower half of the surface Dirac cone is expected to be a weaker bulk-degenerate resonance state. (e) The two dimensionality of the surface state is visible in k_z dependence of the cut 2 Fermi surface. (f),(g) An ARPES cut along the $\bar{M}$-$\bar{X}$-$\bar{M}$ direction. The energy step in (g) is 5 meV. All measurements were performed at $T = 20$ K.

The photon energy was set to $h\nu = 70$ eV, corresponding to a bulk Γ plane of the cubic Brillouin zone (see Supplemental Material, Note 8 [18] for other photon energies). Energy resolution was $\delta E \lesssim 10$ meV, and momentum resolution along the dispersive axis of measurement was $\delta k < 3 \times 10^{-3}$ Å^{-1}. Measurements of k_z dependence for $Sm_{0.7}Ce_{0.3}B_6$ were performed at the NSLS-II ESM beamline, under approximately the same conditions. Samples were cleaved *in situ* at $T \sim 20$ K, using a top post glued to the (001) surface. All ARPES data were taken within 10 h after cleavage, and band structure near the Fermi level was stable on this timescale (Supplemental Material, Note 3 [18]). Additional method details for resistivity and magnetic susceptibility measurements are described in the Supplemental Material (Note 4 [18]).

There are conflicting interpretations on whether a complete topological classification of SmB_6 surface states has been achieved [45–47], particularly with respect to weakly visible Fermi surfaces surrounding the Brillouin zone center. However, measurements consistently show a single surface state Fermi surface surrounding the surface $\bar{X}$ point, with a contour that is not greatly influenced by surface termination [7–12,45–47]. Spin-resolved investigations

have found this state to be singly degenerate [12,48,49], creating a topologically nontrivial surface state (TSS) scenario along the $\bar{X}$-$\bar{M}$ axis [see Fig. 1(d) diagram and Supplemental Material, Note 5 [18]].

High-resolution ARPES experiments were performed on $Sm_{0.7}Ce_{0.3}B_6$ and $Sm_{0.8}Eu_{0.2}B_6$ to address the question of how this topological surface state responds to the altered chemical environments. For $Sm_{0.7}Ce_{0.3}B_6$, low-temperature ($T = 20$ K) measurements show a four-pocket Fermi surface with a long elliptical orientation along the $\bar{\Gamma}$-$\bar{X}$ axis, where the Fermi momentum is marginally closer to $\bar{\Gamma}$ than to $\bar{X}$ [Fig. 1(a)]. These states are two-dimensional [Fig. 1(e); see also Supplemental Material, Note 8 [44]] and qualitatively identical to the $\bar{X}$-point surface state Fermi surface observed at low-temperature for undoped SmB_6. Fermi pockets surrounding the $\bar{\Gamma}$ point are not seen, as is often the case for undoped SmB_6 under the same measurement conditions [10,11]. Examining band dispersions along the $\bar{\Gamma}$-$\bar{X}$ axis reveals steeply sloped bulk states [black dashed lines in Fig. 1(c)] from the $\bar{X}$-point $5d$ pocket, which merge with a flatband associated with $4f$ states. At the Fermi level, there is no feature at the extrapolated Fermi momentum of the $5d$ bulk bands [~ 0.17 Å^{-1} for Fig. 1(c) and ~ 0.41 Å^{-1} for Fig. 1(g)], indicating a well-defined bulk hybridization gap. The gap is crossed by highly dispersive surface states that are offset in momentum from the lower dispersion of the $5d$ band [see guides to the eye in Fig. 1(c)] as is typically seen for undoped SmB_6. A similar scenario is seen along the $\bar{X}$-$\bar{M}$ axis [Fig. 1(g)], with only a single surface state intersecting the Fermi level as required for the topological insulator state attributed to SmB_6.

The same features are seen in $Sm_{0.8}Eu_{0.2}B_6$ [Figs. 2(a) and 2(b)], however, we find that the bulk electron pocket contours have shifted away from the Brillouin zone center by $\Delta k = 0.07$ Å^{-1} relative to $Sm_{0.7}Ce_{0.3}B_6$. If taken to represent an isotropic fractional change in Fermi momentum, this indicates the addition of 0.2 holes per unit cell in the $5d$ orbital. This difference in the bulk electronic structures can be understood by noting that the samarium sites in SmB_6 are mixed valent with a roughly equal mixture of $4f^5$ and $4f^6$ configurations [50], whereas cerium and europium have strongly favored f-shell occupancies of $4f^1$ (Ce^{3+}) and $4f^7$ (Eu^{2+}) [51,52] (see characterization in Supplemental Material, Note 6 [18]) and can be expected to contribute $\sim 50\%$ fractional electron (Ce^{3+}) and hole (Eu^{2+}) doping, respectively, to the samarium sublattice. The observed difference in bulk $5d$ dispersions accounts for roughly 80% of this nominal doping effect, suggesting that most of the doped charge resides in itinerant $5d$ states, with just a few percent ($< \sim 5\%$) of an electron or hole doped into the strongly correlated Sm $4f$ sublattice.

Raising the temperature of $Sm_{0.8}Eu_{0.2}B_6$ from 10 to 180 K shows incremental broadening and a downward energetic shift of the flat $4f$ state [Fig. 2(b)], as is also seen for undoped
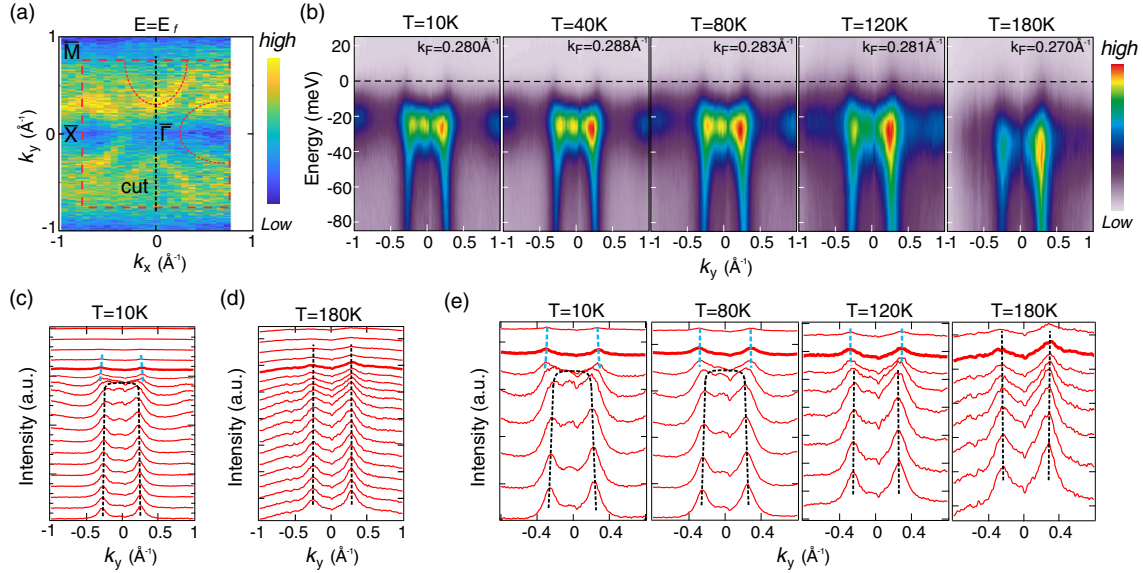
FIG. 2. Surface state emergence after 20% Eu doping. (a) The Fermi surface of $Sm_{0.8}Eu_{0.2}B_6$. (b) A low-energy ARPES cut taken along the high-symmetry $\bar{X}$-$\bar{\Gamma}$-$\bar{X}$ direction [traced in (a)] is shown as a function of temperature and annotated with the momentum-axis center of mass of Fermi level features. Raw data underlying the $T = 10$ (c) and 180 K (d) images are traced with surface (blue) and bulk (black) bands. The Fermi level is indicated with a thicker line, and the energy step is 6 meV. (e) Raw data curves within 50 meV of the Fermi level are shown for selected temperatures, with an energy step of 7 meV.

SmB_6 [8,11]. The Fermi momentum of the in-gap feature declines at $T > 120$ K [see Fig. 2(b)], as the surface state (with larger Fermi momentum) vanishes and is replaced within the incoherent Kondo gap by a continuation of the bulk $5d$ state [see Fig. 2(e) progression]. The similarity of the low-temperature Fermi level band structure in these highly doped configurations is remarkable, but consistent with recent theory for mixed-valent systems [53] and with a majority of doped electrons occupying the itinerant $5d$ states as attributed above.

Unlike these topological features, local moment physics and many-body ordering energetics cannot be unaffected by magnetic doping. As Ce doping level increases, the magnetic susceptibility (χ-T) curves evolve rapidly and nonlinearly to strongly resemble the CeB_6 curve after just 30% substitution [Fig. 3(a)]. Fitting inverse susceptibility ($1/\chi$-T) with a Curie-Weiss function in the high-temperature paramagnetic regime (Supplemental Material, Note 7 [18]) reveals effective local moments of 5.4 μ_B ($Sm_{0.99}Ce_{0.01}B_6$), 5.15 μ_B ($Sm_{0.97}Ce_{0.03}B_6$), 4.2 μ_B ($Sm_{0.9}Ce_{0.1}B_6$), and 3.15 μ_B ($Sm_{0.7}Ce_{0.3}B_6$). The terminal value at 30% doping is remarkably close to the local moment of CeB_6, or the free-ion $4f^1$ scenario, both of which are around 2.54 μ_B [54,55].

Large-moment doping with Eu yields a similarly nonlinear trend, but in the opposite direction. Europium gravitates strongly to the half filled large-spin $4f^7$ configuration favored by intra-atomic exchange interactions, with a large effective moment of 8 μ_B in EuB_6 [59]. Partial substitution of samarium as $Sm_{1-x}M_xB_6$ induces antiferromagnetic order [60], which can be seen from the susceptibility kinks at

$T = 2.8$ K ($Sm_{0.9}Eu_{0.1}B_6$) and $T = 7$ K ($Sm_{0.8}Eu_{0.2}B_6$) in Fig. 3(b). The effective moments extracted from inverse susceptibility for Eu-alloyed SmB_6 are 4.2 μ_B ($Sm_{0.95}Eu_{0.05}B_6$), 7.1 μ_B ($Sm_{0.9}Eu_{0.1}B_6$), and 6.1 μ_B ($Sm_{0.8}Eu_{0.2}B_6$). The rapid change in local moments may be aided by a complementary effect from charge doping. Electron doping from Ce is expected to reduce local moment by promoting occupancy of the zero-moment ($^7F_0$) multiplet ground state of $4f^6$ Sm, and hole doping from Eu will have the opposite effect by biasing the system toward large-moment $4f^5$ configurations.

Transport trends are also very different between the Ce- and Eu-alloyed samples. The resistivity of undoped SmB_6 is strikingly enhanced beneath the Kondo onset of $T \sim$ 50 K [Fig. 3(c)], before flattening into a plateau associated with surface state conductivity [13,61,62] at T < 10 K. Substituting 3% Sm with Ce causes $T \lesssim 5$ K bulk resistivity to be reduced by 1–2 of magnitude [Fig. 3(c)], an effect that seems counterintuitive in the context of adding defects, but matches expectations for an insulating Kondo lattice, as impurities may create in-gap states and suppress the coherence of the insulating Kondo band structure [39,63]. The Kondo-regime resistivity of $Sm_{1-x}Ce_xB_6$ is suppressed further at higher doping levels, but retains an upturn beneath $T \lesssim 50$ K. For $Sm_{0.7}Ce_{0.3}B_6$, the trend beneath $T \lesssim 4$ K appears to be metallic (positively sloped), and resembles pure CeB_6 [see Fig. 3(c) inset].

The insulating character of $Sm_{1-x}Eu_xB_6$ [Fig. 3(d)] is far more robust, with a nonmonotonic trend under doping that has been noted in previous literature [60]. The alloys retain a characteristic Kondo insulating exponential trend (see
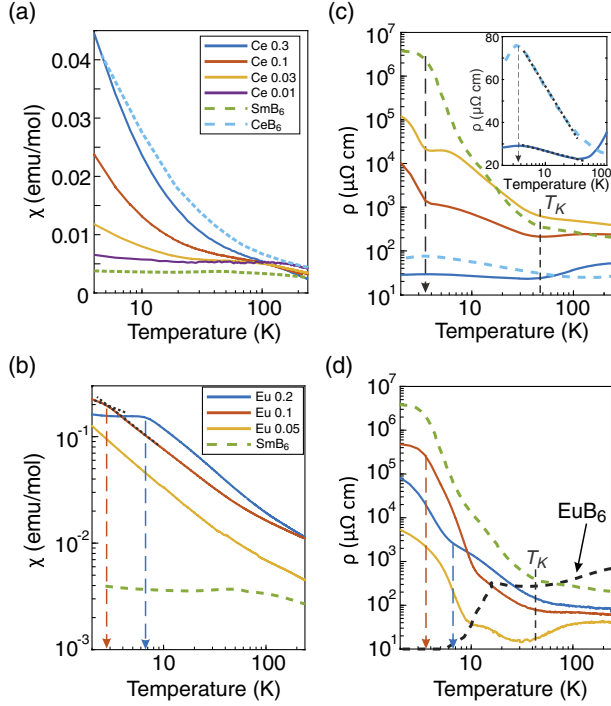
FIG. 3. Resistivity and susceptibility of magnetically doped alloys. (a) Magnetic susceptibility of Ce-alloyed SmB_6. Data for pristine CeB_6 and SmB_6 are extracted from Refs. [55,56]. (b) Magnetic susceptibility of Eu-alloyed SmB_6. Drop arrows mark the magnetic transition at 10% and 20% Eu doping levels. (c) Resistivity of Ce-alloyed SmB_6. A black drop arrow marks the onset of the $T < 10$ K surface conductivity plateau for SmB_6, which happens to coincide with bulk-derived resistivity kinks in the alloyed samples. Data for pristine CeB_6 and SmB_6 are extracted from Refs. [57,58], and an inset compares the resistivity trends for CeB_6 and $Sm_{0.7}Ce_{0.3}B_6$. (d) Resistivity of Eu-alloyed SmB_6, with data for pristine EuB_6 extracted from Ref. [59]. Red and blue arrows indicate magnetic transitions, as in (b).
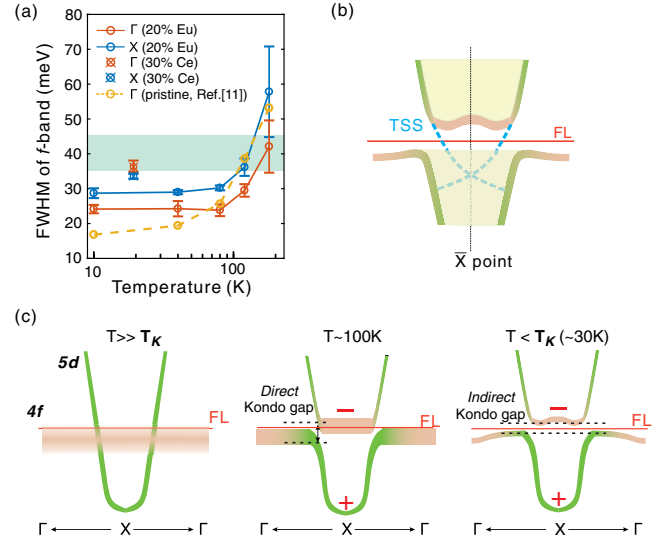

FIG. 4. Coherence, hybridization, and surface state emergence. (a) The $4f$ band feature width at half maximum in alloys is evaluated from a Voigt fit and compared with pristine SmB_6 as a function of temperature. A shaded region indicates the threshold below which surface states become visible to ARPES. (b) A schematic showing surface states spanning the Fermi level (FL) hybridization gap. Bulk states with zero z-axis momentum are drawn as solid lines, and the k_z-projected bulk state continuum is shown with light yellow shading. (c) Diagrams show the temperature-resolved evolution of TKI bulk band structure intersecting the X point. Middle: as coherence increases with the lowering of temperature, topologically inverted direct hybridization gaps open at band crossing points. Right: as temperature decreases further, the presence or absence of an indirect gap within the Kondo band structure defines the trend of resistivity. The topologically inverted parity symmetries are indicated by "$+$" (d orbital) and "$-$" (f orbital) signs.

Supplemental Material, Fig. S9 [18]). Mild inflections of resistivity are seen at the Néel transitions, but are not very distinguishable from other nonlinear details within the plot and differ starkly from the dramatic change caused by ferromagnetism at $T_C \sim 12$ K in EuB_6 [59].

With respect to the trend toward metallicity in Ce alloys, it is intriguing to note that pure CeB_6 also presents a $4f/5d$ Kondo lattice scenario, with a superficially similar onset of Kondo-associated resistivity to SmB_6 at $T \lesssim 50$ K [Fig. 3(c)]. However, the CeB_6 bulk band structure that emerges from low-temperature Kondo coherence is metallic due to the high density of Kondo-active large-moment sites [64], and the modest increase of resistivity as Kondo coherence sets in appears to represent the transition to a low-mobility, heavy-Fermion band structure [65,66]. However, there is no fully established approach to modeling the band structure of a dense Kondo lattice like CeB_6 or a mixed-valent one like SmB_6. Theory for SmB_6 often builds from a computationally tractable single-particle band hybridization picture, however, the monovalent nature

ascribed to cerium in CeB_6 is much less compatible with such a picture, and the coincidence of Kondo temperature scales within resistivity measurements is suggestive that a complete theory for $Sm_{0.7}Ce_{0.3}B_6$ may need to go beyond a single-particle modeling basis.

From an empirical perspective, $Sm_{0.7}Ce_{0.3}B_6$ has superior $T < 50$ K conductivity to pure CeB_6 and preserves the topological surface state of SmB_6, and so appears to be a poor fit for the standard picture in which the metallicity of a disordered Kondo insulator comes from an in-gap impurity band [39]. Examining the low-temperature $4f$ states in greater detail, we find that they are broader along the energy axis than those seen in SmB_6, with a peak width at half maximum (half-width) that is greater by ~ 15–20 meV [Fig. 4(a)]. This change is much larger than the ~ 4 meV insulating gap attributed from the activation of resistivity in SmB_6 [15] and suggests that impurities may close the gap by introducing a broader continuum of diffusively conducting states. Similar $4f$-associated states are seen by ARPES at low temperature in CeB_6, but are much broader [67,68], making it difficult to perform a fine comparison.

As temperature increases, a rapid thermal activation of $4f$ half-width is seen for undoped SmB_6 and $Sm_{0.8}Eu_{0.2}B_6$ at $T \gtrsim 80$ K, and is consistent with the square of temperature (T^2) trend expected for Fermi liquid self-energy. In all cases, surface states and $4f/5d$ hybridization are visible at $4f$ half-width values less than 40 meV, found at temperatures $T \lesssim 120$ K. This phenomenology is consistent with recent theoretical investigations, which have proposed that the topological insulating gap of band insulatorlike TKI systems may be highly robust against defects at the ~20% level [53,69]. This picture may also relate to the lack of surface states in ARPES studies of pure CeB_6 [67,68], which has a $4f$-state width considerably larger than 40 meV.

The picture that emerges is one in which the topological surface states of SmB_6 alloys begin to emerge in concert with the direct $4f/5d$ hybridization gap as coherence improves at $T \lesssim 120$ K. This matches expectations that the direct Kondo gap will define topology within a band picture [see Fig. 4(c)]. The transition is unlikely to be sudden, as earlier studies on undoped SmB_6 have shown that the bulk bands evolve continuously throughout the onset of f-electron coherence [11]. Surface states satisfy a nontrivial topology along the X-M axis and are found near the outer boundary of the k_z-projected $5d$ state continuum [Fig. 4(b)]. The robustness of both surface states and the gap are remarkable given that SmB_6 may otherwise be unique as a TKI and may be due to the unusual tendency of Sm toward *mixed-valent* electronic configurations [53,69] (see further discussion at the end of the Supplemental Material, Note 2 [18]). Moreover, the crossover to a metallic (positively sloped) low-temperature resistivity trend appears to relate to changes in the band structure on a smaller energy scale comparable to the ~4 meV indirect band gap.

Taken collectively, these results show that TKI surface states can still emerge in alloys that deviate greatly from the parent compound SmB_6 in terms of metallicity, magnetic local moment, and magnetic ground state. This will enable the exploration of TKI surface physics in new physical regimes and supports recent theoretical modeling, which has suggested that topological band gap and surface state properties of SmB_6-like TKI materials will be far more robust against disorder than is typically expected for Kondo lattice systems [53,69]. Comparing these alloys with undoped SmB_6 and CeB_6, the emergence of TKI surface states is found to consistently coincide with the opening of a direct band gap in the bulk $5d$ spectral function, which in turn is associated with $4f$-state half-widths falling beneath a critical $\lesssim 40$ meV threshold. Local moments are seen to vary by a factor of 2, from roughly 3.15 μ_B in $Sm_{0.7}Ce_{0.3}B_6$ to over 6 μ_B in $Sm_{1-x}Eu_xB_6$ ($x = 0.1,\ 0.2$), and the differing $4f$-electron energetics appear to result in contrasting trends toward metallic- and insulatinglike Kondo lattice scenarios for Ce and Eu alloys, respectively. The insulatinglike scenario realized by $Sm_{0.8}Eu_{0.2}B_6$

places topological surface states at the Fermi level in a system with $T_N = 7$ K antiferromagnetism, presenting a remarkably clean candidate system for the much-sought antiferromagnetic topological insulator state.

---

*Corresponding author.
lawray@nyu.edu

[1] A. Menth, E. Buehler, and T. H. Geballe, Magnetic and Semiconducting Properties of SmB_6, Phys. Rev. Lett. **22,** 295 (1969).

[2] R. L. Cohen, M. Eibschütz, and K. W. West, Electronic and Magnetic Structure of SmB_6, Phys. Rev. Lett. **24,** 383 (1970).

[3] M. Dzero, J. Xia, V. Galitski, and P. Coleman, Topological Kondo insulators, Annu. Rev. Condens. Matter Phys. **7,** 249 (2016).

[4] M. Dzero, K. Sun, V. Galitski, and P. Coleman, Topological Kondo Insulators, Phys. Rev. Lett. **104,** 106408 (2010).

[5] M. Dzero, K. Sun, P. Coleman, and V. Galitski, Theory of topological Kondo insulators, Phys. Rev. B **85,** 045130 (2012).

[6] F. Lu, J. Z. Zhao, H. Weng, Z. Fang, and X. Dai, Correlated Topological Insulators with Mixed Valence, Phys. Rev. Lett. **110,** 096401 (2013).

[7] M. Neupane, N. Alidoust, S-Y. Xu, T. Kondo, Y. Ishida, D. J. Kim, C. Liu, I. Belopolski, Y. J. Jo, T.-R. Chang, H.-T. Jeng, T. Durakiewicz, L. Balicas, H. Lin, A. Bansil, S. Shin, Z. Fisk, and M. Z. Hasan, Surface electronic structure of the topological Kondo-insulator candidate correlated electron system SmB_6, Nat. Commun. **4,** 2991 (2013).

[8] J. Jiang, S. Li, T. Zhang, Z. Sun, F. Chen, Z. R. Ye, M. Xu, Q. Q. Ge, S. Y. Tan, X. H. Niu, M. Xia, B. P. Xie, Y. F. Li, X. H. Chen, H. H. Wen, and D. L. Feng, Observation of possible topological in-gap surface states in the Kondo

insulator SmB$_6$ by photoemission, Nat. Commun. **4**, 3010 (2013).

[9] N. Xu, X. Shi, P. K. Biswas, C. E. Matt, R. S. Dhaka, Y. Huang, N. C. Plumb, M. Radović, J. H. Dil, E. Pomjakushina, K. Conder, A. Amato, Z. Salman, D. McK. Paul, J. Mesot, H. Ding, and M. Shi, Surface and bulk electronic structure of the strongly correlated system SmB$_6$ and implications for a topological Kondo insulator, Phys. Rev. B **88**, 121102(R) (2013).

[10] J. D. Denlinger, J. W. Allen, J.-S. Kang, K. Sun, B-I. Min, D.-J. Kim, and Z. Fisk, SmB$_6$ photoemission: Past and present, JPS Conf. Proc. **3**, 017038 (2014).

[11] J. D. Denlinger, J. W. Allen, J.-S. Kang, K. Sun, J.-W. Kim, J. H. Shim, B. I. Min, D.-J. Kim, and Z. Fisk, Temperature dependence of linked gap and surface state evolution in the mixed valent topological insulator SmB$_6$, arXiv:1312.6637.

[12] Y. Ohtsubo, Y. Yamashita, K. Hagiwara, S. Ideta, K. Tanaka, R. Yukawa, K. Horiba, H. Kumigashira, K. Miyamoto, T. Okuda, W. Hirano, F. Iga, and S. Kimura, Non-trivial surface states of samarium hexaboride at the (111) surface, Nat. Commun. **10**, 2298 (2019).

[13] D.-J. Kim, J. Xia, and Z. Fisk, Topological surface state in the Kondo insulator samarium hexaboride, Nat. Mater. **13**, 466 (2014).

[14] B. Y. Kang, C.-H. Min, S. S. Lee, M. S. Song, K. K. Cho, and B. K. Cho, Magnetic and nonmagnetic doping dependence of the conducting surface states in SmB$_6$, Phys. Rev. B **94**, 165102 (2016).

[15] Y. S. Eo, A. Rakoski, J. Lucien, D. Mihaliov, C. Kurdak, P. F. S. Rosa, and Z. Fisk, Transport gap in SmB$_6$ protected against disorder, Proc. Natl. Acad. Sci. U.S.A. **116**, 12638 (2019).

[16] X.-L. Qi and S.-C. Zhang, Topological insulators and superconductors, colloquium: Topological insulators, Rev. Mod. Phys. **83**, 1057 (2011).

[17] M. Z. Hasan and C. L. Kane, Colloquium: Topological insulators, Rev. Mod. Phys. **82**, 3045 (2010).

[18] See Supplemental Material at http://link.aps.org/supplemental/10.1103/PhysRevLett.126.136401 for additional technique and characterization details, which includes Refs. [19–36].

[19] J. M. Lawrence, T. Graf, M. F. Hundley, D. Mandrus, J. D. Thompson, A. Lacerda, M. S. Torikachvili, J. L. Sarrao, and Z. Fisk, Kondo hole behavior in Ce$_{0.97}$La$_{0.03}$Pd$_3$, Phys. Rev. B **53**, 12559 (1996).

[20] M. H. Hamidian et al., How Kondo-holes create intense nanoscale heavy-fermion hybridization disorder, Proc. Natl. Acad. Sci. U.S.A. **108**, 18233 (2011).

[21] P. F. S. Rosa, A. Oostra, J. D. Thompson, P. G. Pagliuso, and Z. Fisk, Unusual Kondo-hole effect and crystal-field frustration in Nd-doped CeRhIn$_5$, Phys. Rev. B **94**, 045101 (2016).

[22] H. He et al., Irreversible proliferation of magnetic moments at cleaved surfaces of the topological Kondo insulator SmB$_6$, Phys. Rev. B **95**, 195126 (2017).

[23] P. Lutz, M. Thees, T. R. F. Peixoto, B. Y. Kang, B. K. Cho, C. H. Min, and F. Reinert, Valence characterisation of the subsurface region in SmB$_6$, Philos. Mag. **96**, 3307 (2016).

[24] S. Suga et al., Spin-polarized angle-resolved photoelectron spectroscopy of the so-predicted Kondo topological insulator SmB$_6$, J. Phys. Soc. Jpn. **83**, 014705 (2014).

[25] L. Fu, C. L. Kane, and E. J. Mele, Topological Insulators in Three Dimensions, Phys. Rev. Lett. **98**, 106803 (2007).

[26] F. Siek et al., Angular momentum-induced delays in solid-state photoemission enhanced by intra-atomic interactions, Science **357**, 1274 (2017).

[27] S. Röler, T.-H. Jang, D.-J. Kim, L. H. Tjeng, Z. Fisk, F. Steglich, and S. Wirth, Hybridization gap and Fano resonance in SmB$_6$, Proc. Natl. Acad. Sci. U.S.A. **111**, 4798 (2014).

[28] C. E. Matt et al., Consistency between ARPES and STM measurements on SmB$_6$, Phys. Rev. B **101**, 085142 (2020).

[29] J. A. Colón Santana, J. M. An, N. Wu, K. D. Belashchenko, X. Wang, P. Liu, J. Tang, Y. Losovyj, I. N. Yakovkin, and P. A. Dowben, Effect of gadolinium doping on the electronic band structure of europium oxide, Phys. Rev. B **85**, 014406 (2012).

[30] Hartree-Fock Slater Condon parameters were obtained from the COWAN code (see https://www.tcd.ie/Physics/people/Cormac.McGuinness/Cowan/).

[31] E. Anderson et al., LAPACK User's Guide, 3rd ed. (SIAM, Philadelphia, 1999).

[32] A. Maurya, R. Kulkarni, A. Thamizhavel, D. Paudyal, and S. K. Dhar, Kondo lattice and antiferromagnetic behavior in quaternary CeTAl$_4$Si$_2$ (T = Rh, Ir) single crystals, J. Phys. Soc. Jpn. **85**, 034720 (2016).

[33] Y. Singh, R. S. Sannabhadti, and S. Ramakrishnan, Low-temperature properties of a new Kondo lattice compound Yb$_2$Ir$_3$Sn$_5$, arXiv:cond-mat/0510583.

[34] F. Gerken, Calculated photoemission spectra of the $4f$ states in the rare-Earth metals, J. Phys. F **13**, 703 (1983).

[35] M. Liu et al., Crossover between Weak Antilocalization and Weak Localization in a Magnetically Doped Topological Insulator, Phys. Rev. Lett. **108**, 036805 (2012).

[36] Y. Xu, J. Chiu, L. Miao, H. He, Z. Alpichshev, A. Kapitulnik, R. R. Biswas, and L. Andrew Wray, Disorder enabled band structure engineering of a topological insulator surface, Nat. Commun. **8**, 14081 (2017).

[37] J. D. Thompson, Holes in a Kondo lattice, Proc. Natl. Acad. Sci. U.S.A. **108**, 18191 (2011).

[38] R. Sollie and P. Schlottmann, A simple theory of the Kondo hole, J. Appl. Phys. **69**, 5478 (1991).

[39] P. Schlottmann and C. S. Hellberg, Metal-insulator transition in dirty Kondo insulators, J. Appl. Phys. **79**, 6414 (1996).

[40] R. S. K. Mong, A. M. Essin, and J. E. Moore, Antiferromagnetic topological insulators, Phys. Rev. B **81**, 245209 (2010).

[41] J. Li, Y. Li, S. Du, Z. Wang, B.-L. Gu, S.-C. Zhang, K. He, W. Duan, and Y. Xu, Intrinsic magnetic topological insulators in van der Waals layered MnBi$_2$Te$_4$-family materials, Sci. Adv. **5**, eaaw5685 (2019).

[42] C. Sanchez-Castro, P. Bedell, and B. Cooper, Hybridization gap insulating behavior of Ce$_3$Bi$_4$Pt$_3$, Phys. Rev. B **47**, 6879 (1993).

[43] B. Bucher, Z. Schlesinger, P. C. Canfield, and Z. Fisk, Kondo Coupling Induced Charge Gap in Ce$_3$Bi$_4$Pt$_3$, Phys. Rev. Lett. **72**, 522 (1994).

[44] N. S. Vidhyadhiraja and D. E. Logan, Optical and transport properties of heavy fermions, J. Phys. Condens. Matter **17**, 2959 (2005).

[45] Z.-H. Zhu, A. Nicolaou, G. Levy, N. P. Butch, P. Syers, X. F. Wang, J. Paglione, G. A. Sawatzky, I. S. Elfimov, and A. Damascelli, Polarity-Driven Surface Metallicity in SmB_6, Phys. Rev. Lett. **111,** 216402 (2013).

[46] E. Frantzeskakis, N. de Jong, B. Zwartsenberg, Y. K. Huang, Y. Pan, X. Zhang, J. X. Zhang, F. X. Zhang, L. H. Bao, O. Tegus, A. Varykhalov, A. de Visser, and M. S. Golden, Kondo Hybridization and the Origin of Metallic States at the (001) Surface of SmB_6, Phys. Rev. X **3,** 041024 (2013).

[47] P. Hlawenka, K. Siemensmeyer, E. Weschke, A. Varykhalov, J. Sánchez-Barriga, N. Y. Shitsevalova, A. V. Dukhnenko, V. B. Filipov, S. Gabáni, K. Flachbart, O. Rader, and E. D. L. Rienks, Samarium hexaboride is a trivial surface conductor, Nat. Commun. **9,** 517 (2018).

[48] N. Xu, P. K. Biswas, J. H. Dil, R. S. Dhaka, G. Landolt, S. Muff, C. E. Matt, X. Shi, N. C. Plumb, M. Radović, E. Pomjakushina, K. Conder, A. Amato, S. V. Borisenko, R. Yu, H.-M. Weng, Z. Fang, X. Dai, J. Mesot, H. Ding, and M. Shi, Direct observation of the spin texture in SmB_6 as evidence of the topological Kondo insulator, Nat. Commun. **5,** 4566 (2014).

[49] N. Xu, H. Ding, and M. Shi, Spin- and angle-resolved photoemission on the topological Kondo insulator candidate: SmB_6, J. Phys. Condens. Matter **28,** 363001 (2016).

[50] J. C. Nickerson, R. M. White, K. N. Lee, R. Bachmann, T. H. Geballe, and G. W. Hull, Jr., Physical properties of SmB_6, Phys. Rev. B **3,** 2030 (1971).

[51] M. Magnuson, S. M. Butorin, J.-H. Guo, A. Agui, J. Nordgren, H. Ogasawara, A. Kotani, T. Takahashi, and S. Kunii, Electronic-structure investigation of CeB_6 by means of soft-x-ray scattering, Phys. Rev. B **63,** 075101 (2001).

[52] Y. Takakuwa, S. Suzuki, and T. Sagawa, Photoemission measurements of EuB_6, Jpn. J. Appl. Phys. **17,** 284 (1978).

[53] B. Skinner, Properties of the donor impurity band in mixed valence insulators, Phys. Rev. Mater. **3,** 104601 (2019).

[54] S. Blundell, *Magnetism in Condensed Matter* (Oxford University Press, Oxford, 2001), .

[55] C. Terzioglu, D. A. Browne, R. G. Goodrich, A. Hassan, and Z. Fisk, EPR and magnetic susceptibility measurements on CeB_6, Phys. Rev. B **63,** 235110 (2001).

[56] M. C. Hatnean, M. R. Lees, D. M. Paul, and P. G. Balakrishnan, Large, high quality single-crystals of the new topological Kondo insulator, SmB_6, Sci. Rep. **3,** 3071 (2013).

[57] T. Fujita, M. Suzuki, T. Komatsubara, S. Kunii, T. Kasuya, and T. Ohtsuka, Anomalous specific heat of CeB_6, Solid State Commun. **35,** 569 (1980).

[58] X. Zhang, N. P. Butch, P. Syers, S. Ziemak, R. L. Greene, and J. Paglione, Hybridization, Inter-Ion Correlation, and Surface States in the Kondo Insulator SmB_6, Phys. Rev. X **3,** 011011 (2013).

[59] S. Süllow, I. Prasad, M. C. Aronson, J. L. Sarrao, Z. Fisk, D. Hristova, A. H. Lacerda, M. F. Hundley, A. Vigliante, and D. Gibbs, Structure and magnetic order of EuB_6, Phys. Rev. B **57,** 5860 (1998).

[60] S. Yeo, K. Song, N. Hur, Z. Fisk, and P. Schlottmann, Effects of Eu doping on SmB_6 single crystals, Phys. Rev. B **85,** 115125 (2012).

[61] S. Wolgast, C. Kurdak, K. Sun, J. W. Allen, D.-J. Kim, and Z. Fisk, Low-temperature surface conduction in the Kondo insulator SmB_6, Phys. Rev. B **88,** 180405(R) (2013).

[62] D. J. Kim, S. Thomas, T. Grant, J. Botimer, Z. Fisk, and Jing Xia, Surface Hall effect and nonlocal transport in SmB_6: Evidence for surface conduction, Sci. Rep. **3,** 3150 (2013).

[63] S. Wermbter, K. Sabel, and G. Czycholl, Electrical resistivity of heavy-fermion systems with nonmagnetic impurities, Phys. Rev. B **53,** 2528 (1996).

[64] J. M. Effantin, J. Rossat-Mignod, and P. Burlet, Magnetic phase diagram of CeB_6, J. Magn. Magn. Mater. **47–48,** 145 (1985).

[65] S. Nakatsuji, D. Pines, and Z. Fisk, Two Fluid Description of the Kondo Lattice, Phys. Rev. Lett. **92,** 016401 (2004).

[66] P. Coleman, Heavy fermions and the Kondo lattice: A 21st century perspective, in *Many-Body Physics: From Kondo to Hubbard*, edited by E. Pavarini, E. Koch, and P. Coleman (Forschungszentrum Jülich, Jülich, Germany, 2015), Chap. 1, pp. 1.1–1.34.

[67] M. Neupane, N. Alidoust, I. Belopolski, G. Bian, S.-Y. Xu, D.-J. Kim, P. P. Shibayev, D. S. Sanchez, H. Zheng, T.-R. Chang, H.-T. Jeng, P. S. Riseborough, H. Lin, A. Bansil, T. Durakiewicz, Z. Fisk, and M. Zahid Hasan, Fermi surface topology and hot spot distribution in the Kondo lattice system CeB_6, Phys. Rev. B **92,** 104420 (2015).

[68] S. V. Ramankuttya, N. de Jonga, Y. K. Huanga, B. Zwartsenberga, F. Massee b, T. V. Baya, M. S. Goldena, and E. Frantzeskakis, Comparative study of rare earth hexaborides using high resolution angle-resolved photoemission, J. Electron Spectrosc. Relat. Phenom. **208,** 43 (2016).

[69] P. P. Baruselli and M. Vojta, Kondo holes in topological Kondo insulators: Spectral properties and surface quasiparticle interference, Phys. Rev. B **89,** 205105 (2014).